Facile Fabrication of Near-Infrared-Resonant and Magnetic Resonance Imaging-Capable Nanomediators for Photothermal Therapy

Hongwei Chen,*[,‡,#] Xiaoqing Ren,[†,‡,#] Hayley J. Paholak,[‡] Joseph Burnett,[‡] Feng Ni,[‡,§] Xiaoling Fang,[†] and Duxin Sun*[,‡]

[†]Key Laboratory of Smart Drug Deliver, Ministry of Education, Department of Pharmaceutics, School of Pharmacy, Fudan University, 826 Zhangheng Rd., Shanghai 201203, People's Republic of China

[‡]Department of Pharmaceutical Sciences, College of Pharmacy, University of Michigan, 428 Church Street, Ann Arbor, Michigan 48109, United States

[§]Fujian Health College, Fuzhou, Fujian 350101, People's Republic of China

S *Supporting Information*

ABSTRACT: Although many techniques exist for fabricating near-infrared (NIR)-resonant and magnetic resonance imaging (MRI)-capable nanomediators for photothermal cancer therapy, preparing them in an efficient and scalable process remains a significant challenge. In this report, we exploit one-step siloxane chemistry to facilely conjugate NIR-absorbing satellites onto a well-developed polysiloxane-containing polymer-coated iron oxide nanoparticle (IONP) core to generate dual functional core−satellite nanomediators for photothermal therapy. An advantage of this nanocomposite design is the variety of potential satellites that can be simply attached to impart NIR resonance, which we demonstrate using NIR-resonant gold sulfide nanoparticles (Au$_2$SNPs) and the NIR dye IR820 as two example satellites. The core−satellite nanomediators are fully characterized by using absorption spectra, dynamic light scattering, ζ potential measurements, and transmission electron microscopy. The enhanced photothermal effect under the irradiation of NIR laser light is identified through in vitro solutions and in vivo mice studies. The MRI capabilities as contrast agents are demonstrated in mice. Our data suggest that polysiloxane-containing polymer-coated IONPs can be used as a versatile platform to build such dual functional nanomediators for translatable, MRI-guided photothermal cancer therapy.

KEYWORDS: *nanocomposite, surface modification, MRI, photothermal therapy, copolymer, siloxane*
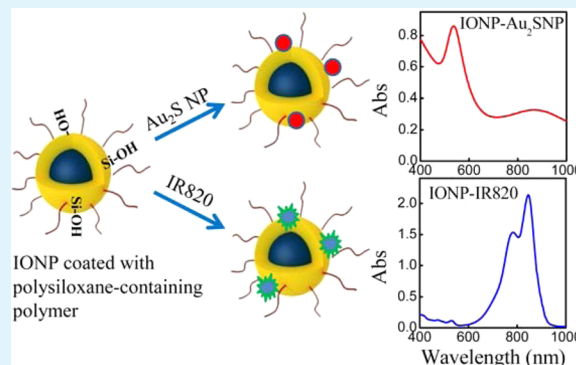
1. INTRODUCTION

Photothermal therapy (PTT) employing near-infrared (NIR)-absorbing nanoparticles, as a minimally invasive and highly effective cancer treatment approach, has gained great attention in recent years.[1−5] Moreover, PTT has been recently combined with immune adjuvant enhanced cancer immunotherapy to harness the immune cells (e.g., T-cells) to fight against both primary and metastatic tumors.[6−9] To improve the efficacy of PTT for cancer treatment, tremendous effort has been devoted to exploring various types of photothermal agents.[10−20] Among them, it is highly desired to develop theranostic nanomediators containing both magnetic and NIR-resonant components to enable simultaneous tumor localization and monitoring of the PTT therapeutic effect noninvasively.[17−23]

Traditional designs for such MRI-capable nanomediators of PTT have been focused on building gold (Au) nanoshells around magnetic nanoparticle cores.[17−20] Ji et al., for instance, reported a multistep procedure for fabricating IONP-Au nanoshells.[18] The magnetic nanoparticles were first coated with amorphous silica via the sol−gel process using tetraethylorthosilicate (TEOS) as a precursor, and then the silica surface was functionalized with amine groups in order to attach Au nanocrystal seeds (2−3 nm). Finally the attached Au nanoseeds were used to nucleate the growth of an Au outlayer to form an Au nanoshell. To tune the nanomediator absorption to the NIR range, the thickness of the Au nanoshell has to be strictly controlled. Later, Zhang et al. reported a sequential process involving sol−gel, surface-protected etching and seed-mediated processes to fabricate superparamagnetic Au nanoshells to improve the reproducibility and structural stability.[19] To simplify the multistep synthesis, Dong et al. reported a facile strategy to make dual functional magnetic core/gold shell-

structured nanocomposites.[17] Instead of using the sol−gel process to make a silica layer, magnetic nanoparticles were encapsulated with amphiphilic block copolymers (polystyrene-b-poly(acrylic acid)) followed by cross-linking with 3-mercaptopropyltrimethoxysilane (MPTMS) in order to attach Au nanoseeds which grow to form an Au nanoshell. However, multiple-step synthesis is needed to make these imaging-capable nanomediators, which could limit their wide applications. Furthermore, the average diameter of the resultant nanomediators is usually in the range of 120−150 nm, which is larger than the ideal size range to maximize exploitation of the enhanced permeability and retention (EPR) effect.[24]

In addition to fabricating Au nanoshells containing a magnetic core to develop MRI-capable and NIR-resonant nanomediators, an alternative strategy was to incorporate NIR-absorbing organic dyes into a magnetic nanoparticle system.[25−29] Ma et al., for instance, produced a nanocomposite that can induce intense temperature elevation and tumor ablation upon NIR laser irradiation by loading indocyanine green (ICG) into phospholipid-PEG coated IONPs.[28] However, physical encapsulation of the NIR dye may make it difficult to maintain stability in the bloodstream, given that the reported nanomediator was administered by intratumor injection instead of systemically. In addition, the loading efficiency is relatively low due to limited space in the nanomediator core that is additionally occupied by the magnetic nanoparticle.

Therefore, it is highly desired to develop an effective yet facile strategy to fabricate dual functional nanomediators for imaging-capable photothermal cancer therapy. Very recently, magnetic nanoparticles coated with a NIR-resonant CuS shell or the light-absorbing polymer polypyrrole were reported.[30,31] In line with these great efforts we use a well-developed polysiloxane-containing polymer coated-IONP core and a variety of NIR-absorbing satellites to facilely fabricate NIR-resonant, MRI-capable nanomediators, for which we demonstrate effective heating and imaging tumors in mice with triple-negative breast cancer. We and others have reported various biomedical applications of these polysiloxane-containing polymer-coated IONPs, including their use as an MRI contrast agent.[32−38] One of the unique properties of the polysiloxane-containing polymer coating is that the surface can be easily modified through siloxane-containing compounds (e.g., MPTMS).[35] In this report, we use both inorganic (e.g., gold sulfide nanoparticles) and organic materials (e.g., IR820 dye) for NIR-resonant components to decorate polysiloxane-containing polymer-coated IONPs. Gold sulfide nanoparticles (2−30 nm) (Au_2SNPs) have been recently been studied as photothermal mediators because of their NIR resonant capability and small average size.[15,16,39,40] We further demonstrate that these Au_2SNPs can be effectively attached onto the IONP polymer coating layer through one-step surface modification. In addition, we also prove that IR820 modified with MPTMS could be covalently conjugated onto this versatile IONP platform.

2. MATERIALS AND METHODS

2.1. Materials. Iron oxide(III) (FeO(OH), hydrated, catalyst grade, 30−50 mesh), oleic acid (technical grade, 90%), 1-octadecene (technical grade, 90%), anhydrous tetrahydrofuran (THF, 99.8%), sodium sulfide, chloroauric acid, IR820, 3-mercaptopropyltrimethoxysilane (MPTMS), dimethylformamide (DMF, 99.9%), dimethyl sulfoxide (DMSO, 99.9%), ammonium iron(II) sulfate hexahydrate ($(Fe(NH_4)_2(SO_4)_2.6H_2O$, ACS reagent, 99%), o-phenanthroline monohydrate (ACS reagent, 99%), hydroquinone (ACS reagent, 99%), nitric acid (ACS reagent, 70%), and hydrochloric acid (ACS reagent, 37%) were purchased from Sigma-Aldrich and used directly.

2.2. Synthesis of IONPs Coated with Polysiloxane-Containing Diblock Copolymer. IONPs (15 nm in diameter) were synthesized in organic solvent by thermal decomposition as reported previously.[38] Diblock copolymer (PEO-b-$P_γMPS$) was synthesized by the reversible addition of fragmentation chain transfer (RAFT) polymerization as previously reported.[34] The method for coating single core nanocrystals was reported previously.[38] The average hydrodynamic diameter of resultant water-soluble IONPs was measured using a dynamic light scattering instrument (Malvern Zeta Sizer Nano S-90). The magnetic nanocrystals and core−satellite structure were viewed by transmission electron microscopy (TEM) (Philips CM-100 60 kV). UV−vis−NIR spectra were recorded in a BioTek microplate reader (Synergy 2) using 200 μL of aqueous solution.

2.3. Synthesis of Au_2S Nanoparticles. Au_2SNPs were synthesized by using sodium sulfide (Na_2S) as the reducing reagent as reported before.[16,39] Gold in the form of chloroauric acid ($HAuCl_4$) was prepared to a concentration of 100 mM as a stock solution and was diluted to 2.0 mM before use. Na_2S (50 mM) was prepared and aged in the dark for 40−48 h prior to use and was diluted to 1.0 mM before use. The volume ratio of Na_2S to $HAuCl_4$ was varied from 4.7/5.0 up to 5.1/5.0. UV−vis spectra were recorded to monitor the reaction. The nanoparticles with optimal absorbance in NIR range were selected to use in the following steps.

2.4. Synthesis of IONP-Au_2SNP Nanomediator. To make the core−satellite nanomediator, we first modified IONPs with thiol-containing MPTMS simply by adding 8 μL of MPTMS to 2 mL of polymer-coated IONP solution (iron concentration of 1.8 mg/mL) at room temperature with gentle stirring for 2 days. After this, freshly made Au_2SNP solution (11 mL) was added and left to mix together overnight. The resultant nanomediators were incubated with HS-PEG_{5000} (Creative PEGWorks, Winston-Salem, NC) overnight and then purified by magnet three times at 4 °C to remove unbound Au_2SNPs. Upon removing the supernatant, the concentrated solution was collected and its iron and gold concentrations were measured by inductively coupled plasma optical emission spectrometry (ICP-OES) with yttrium as the internal standard.

2.5. Synthesis of IONP-IR820 Nanomediator. IR820 (174.0 mg) was dissolved in 10 mL of anhydrous DMF in a 50 mL flask and the mixture was purged with N_2 for 1 h. Then 120 μL of MPTMS was added, and the reaction was carried out at room temperature overnight in the dark.[41,42] The resultant mixture was then added into a mixture of diethyl ether/ethanol (v/v: 10/1). The precipitants were washed with ether and then 2.5 mL of DMSO was added to dissolve the pellet. The residue of ether was removed by an evaporator under reduced pressure at room temperature. The freshly made MPTMS-modified IR820 (1.3 mL) was mixed with 5 mL of polymer-coated IONPs in borate buffer (50 mM, pH 8.0) overnight in the dark at room temperature. The resultant system was successively centrifuged at 22 000 rpm for 1 h (Allegra 64R Centrifuge). The supernatant was collected for measuring the unbound IR820 concentration and the pellet was suspended in borate buffer.

Scheme 1. Schematic Illustration of Attaching Gold Sulfide Nanoparticles (Au$_2$SNPs) to Polysiloxane-Containing Polymer-Coated IONP to Facilely Fabricate NIR-Resonant and MRI-Capable Nanomediator
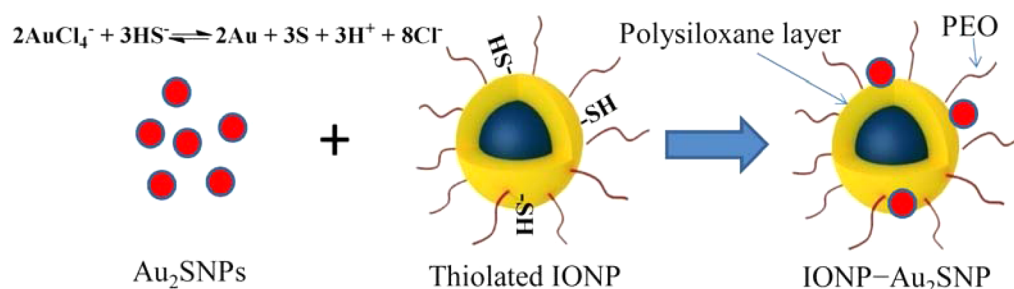
2.6. Photothermal Effect of Core–Satellite Nanomediators in Aqueous Solutions.

To study the nanomediators' photothermal effect induced by NIR light, the aqueous solutions (1.0 mL) of the IONP-Au$_2$SNP or IONP-IR820 nanomediators with a Fe concentration of 0.2 mg/mL in a cuvette were irradiated using a NIR laser (885 nm, spot size, 5 × 8 mm^2, MDL-III-885, OPTO Engine LLC, Midvale, UT) for 10 min with different laser power settings as specified. The temperatures of the solutions were measured by a digital thermometer.

2.7. Cell Culture.

SUM-159 cells were cultured under a 5% CO$_2$ environment in Ham's F-12 media (Invitrogen, Carlsbad, CA) supplemented with 5% fetal bovine serum (Fisher Scientific, Pittsburgh, PA), 1% antibiotic-antimycotic (Invitrogen, Carlsbad, CA), 5 μg/mL insulin (Sigma-Aldrich, St Louis, MO), 1 μg/mL hydrocortisone (Sigma-Aldrich, St Louis, MO), and 4 μg/mL gentamicin (Invitrogen, Carlsbad, CA).

2.8. Xenograft Mouse Model.

All studies involving mice were conducted in accordance with a standard animal protocol approved by the University Committee on the Use and Care of Animals at the University of Michigan. Five week old nude mice were obtained from Charles River Breeding Laboratories. Xenograft formation was generated by direct injection of 1 × 10^6 SUM-159 triple negative breast cancer cells, suspended in matrigel, into the exposed no.4 inguinal mammary pad. Tumor detection was assessed by palpation and, once identified, measurements of tumor volume were carried out using digital calipers and calculated by volume = (width)^2 × length/2.

2.9. Biodistribution.

SUM-159 tumor-bearing nude mice were used for this study. Mice (three mice in each group) were intravenously injected with IONP-Au$_2$SNPs or IONP-IR820 (20 mg Fe/kg mouse body weight) or PBS as a control when tumor sizes reached 5–8 mm. After 24 h, animals were sacrificed. Blood samples were collected by terminal heart puncture and centrifuged for 10 min at 5000 rpm to separate the serum. The tissue samples of tumor, liver, spleen, lungs, kidney, heart, brain, stomach, and muscle were collected and weighed. To determine the iron concentrations in the serum or major organs, 200 μL of serum or whole organ tissue samples were digested in 1 mL of nitric acid or aqua regia (2 mL for liver). After filtration (acrodisc syringe filters, PTFE membrane, diameter 13 mm, pore size 0.45 μm), the volumes of solutions were adjusted to 10.0 mL, the iron and gold concentrations were analyzed using ICP-OES with yttrium as the internal standard.

2.10. In Vitro MRI and T2 Relaxivity Measurements.

Magnetic resonance imaging (MRI) studies were carried out by using a MRI scanner at 7.4-T field strength. For T2 measurements, a multiecho fast spin–echo sequence was used to simultaneously collect a series of data points at different echo times (TE = 15−90 ms with an increment of 15 ms). The T2 relaxation time of each nanoparticle sample was calculated by fitting the decay curve on a pixel-by-pixel basis by using a nonlinear monoexponential algorithm $M(\text{TE}) = M_0 \exp(-\text{TE}_i/\text{T2})$, where TE is the echo time, $M(\text{TE})$ is the MRI signal intensity at which TE is used.

2.11. MRI of Tumor-Bearing Mice.

Mice were placed in a custom-built volume coil (5 cm ID and 8 cm long) and anesthetized using 2% isoflurane delivered via a mask throughout the MRI experiments. Animals were kept warm in the scanner using a circulating water blanket. Tumor-bearing nude mice were scanned with a wrist coil to collect contrast enhanced MRI data 24 h post intravenous injection (IONP-Au$_2$SNP, IONP-IR820, IR820, IONP, and PBS). A T2 weighted fast spin echo sequence was used to obtain T2 relaxometry of the tumor tissue. Typically, field of view (FOV) of 40 × 70 mm, slice thickness of 1 mm was used. The normalized signal intensities of the selected tumor tissues were calculated manually using ImageJ (U.S. National Institutes of Health, Bethesda, Maryland, USA).[37]

2.12. In Vivo Nanomediator Photothermal Effect under the Irradiation of NIR Laser Light.

Tumor-bearing nude mice were randomly allocated into three groups (five mice in each group) when the solid SUM-159 tumors had grown to 5−8 mm. Mice in each group were intravenously injected with IONP-Au$_2$SNPs (20 mg Fe/kg mouse body weight), IONP-IR820 (20 mg Fe/kg mouse body weight), the same amount of IR820 as that in IONP-IR820, IONPs (20 mg Fe/kg mouse body weight), and PBS. Tumors were irradiated 24 h post injection with a diode laser (λ = 885 nm) at a laser power of 0.5 W (laser fluence rate: 1.25 W/cm^2) for 10 min. The highest tumor surface temperature was recorded by an infrared camera (FLIR Systems, i7, Boston, MA) before and after application of the laser.

2.13. Histology.

Mice were humanely euthanized by CO$_2$ inhalation 24 h following a single I.V. bolus dose of nanoparticles. The harvested tissue was formalin-fixed, embedded in paraffin and sectioned. Unstained slides were dewaxed using xylene and rehydrated using graded alcohol. Rehydrated slides were stained with hematoxylin and eosin (H&E staining) for visualization of nucleic acids and cytoplasm.

2.14. Statistical Analysis.

Differences in biodistribution data were analyzed using a two-tailed unpaired Student's t-test, with $p < 0.05$ considered statistically significant.

3. RESULTS AND DISCUSSION

3.1. IONP-Au$_2$SNP Nanomediator for PTT by NIR Laser Irradiation.

3.1.1. Fabrication and Characterization of
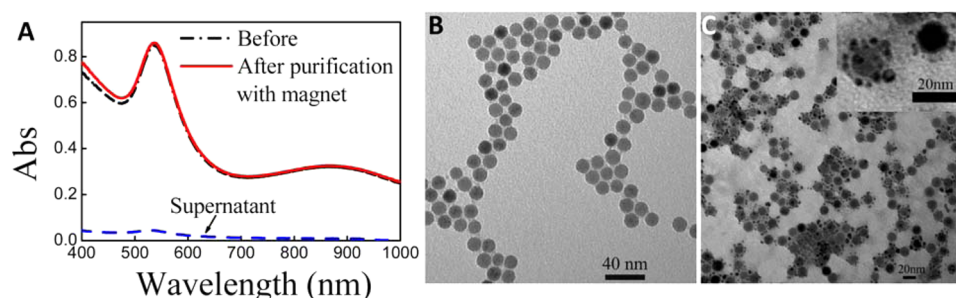
Figure 1. (A) Optical absorption spectrum of IONP-Au$_2$SNP core−satellite nanomediators before and after magnet separation as well as the supernatant. TEM images of polymer-coated IONPs (B) and IONP-Au$_2$SNP core−satellite nanomediators, where the inset shows the zoomed-in image (C).
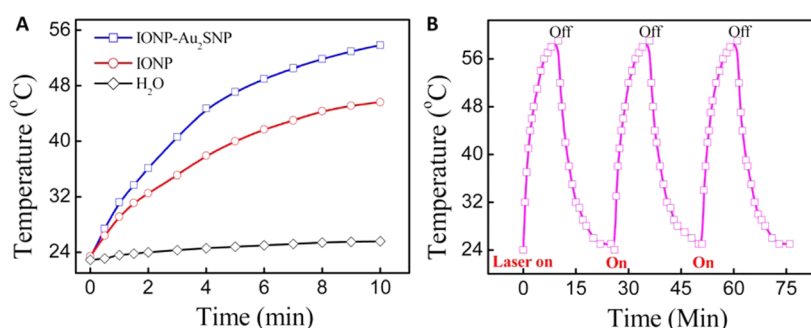

Figure 2. (A) Measured temperatures of IONP-Au$_2$SNP core−satellite nanomediators, IONPs, and water as a control after irradiation with a diode laser (λ = 885 nm) at a laser power of 1.0 W, where both nanoparticle samples have the same Fe concentration at 0.2 mg/mL. (B) Measured temperatures of IONP-Au$_2$SNP core−satellite nanomediators in water with repeated laser on and off, indicating that there is no quenching effect.

IONP-Au$_2$SNP Nanomediator. Developing effective photothermal mediators with MRI capabilities is highly desired because one can locate tumors and monitor therapeutic effects noninvasively.[17−19,23,43] Here, we report a facile way to fabricate MRI-capable photothermal nanomediators by attaching NIR-resonant Au$_2$S nanoparticles onto polysiloxane-containing polymer coated-IONPs as illustrated in Scheme 1 (see Supporting Information Scheme S1 for more information about polysiloxane-containing polymer coating).

Au$_2$SNPs have strong NIR absorption and the NIR peak can be easily controlled from 600 to 900 nm by adjusting the ratio of Na$_2$S/HAuCl$_4$ (Supporting Information Figure S1). Although some controversy continues over the precise structure of these particles,[15,44] their relatively small average size (2−30 nm) and ease of manufacture has garnered interest in their therapeutic applications as traditional photothermal mediators.[16,39,40] By simply mixing freshly made Au$_2$SNPs with thiol-modified IONPs using 3-mercaptopropyltrimethoxysilane (MPTMS), we successfully fabricated IONP-Au$_2$SNP core−satellite nanomediators. Absorption spectra were recorded to monitor the core−satellite assembly process. Our spectra data show that the mixed Au$_2$SNPs are very stable, with no noticeable change of the surface plasmon absorption by comparing spectra of unmixed Au$_2$SNPs with spectra from 20 h and 5 days post mixing with IONPs (Supporting Information Figure S2). The attachment of Au$_2$SNPs onto a single IONP to form core−satellite nanomediators was revealed after applying a magnet to separate any Au$_2$SNPs unbound to IONPs. When applying magnet to the dark red mixture overnight the concentrated pellet is reddish (data not shown), indicating that Au$_2$SNPs are also concentrated by magnet because of binding to IONPs, while the remaining solution (supernatant) becomes colorless. The optical absorption from the resuspended pellet shows obvious absorption characteristic of Au$_2$S nanoparticles as shown in Figure 1a, which is absent from the IONP-only sample (Supporting Information Figure S3) and is identical to the mixture before purification. The absorption spectrum of the supernatant solution (Figure 1a) further confirmed few Au$_2$S nanoparticles are left after purification, revealing the high efficiency of attaching NIR-resonant Au$_2$SNPs onto polysiloxane-containing polymer coated-IONPs.

TEM images of the resultant nanomediator as shown in Figure 1b and 1c clearly illustrate that each bigger nanoparticle (IONP) is surrounded by a few smaller particles (Au$_2$SNPs) (Supporting Information Figure S4). It should be noted that we did observe some scattered triangle-shaped Au$_2$SNPs attached onto IONPs (data not shown), but majority of the satellite particles are spherical. It is estimated that around 10 Au$_2$SNPs are attached to each IONP as shown in the inset of Figure 1c. It is generally believed that these Au$_2$SNPs appear to have a contiguous gold coating, which could potentially allow for the surface conjugation through gold-sulfide interactions to further develop targeted nanoparticles.[16] The hydrodynamic size of the resultant IONP-Au$_2$SNP core−satellite nanomediator with further protection by PEG$_{5000}$ is increased to 57.5 ± 0.2 nm from 23 nm for IONPs (Supporting Information Table S1). Compared to traditional IONP−Au core−shell nanomediators with an average size at ∼150 nm, the core−satellite nanomediator we developed here is much smaller. In addition, the core−satellite nanomediator shows good stability in physiological conditions, as tested in NaCl solution (1.0 M) for over 22 h because of the double protection from the IONP polysiloxane-containing polymer coating and further PEGylation (Supporting Information Figure S5). Taken together with the slightly negative zeta potential (−15.0 ± 0.5 mV), the IONP-Au$_2$SNP core−satellite nanomediator may have reduced
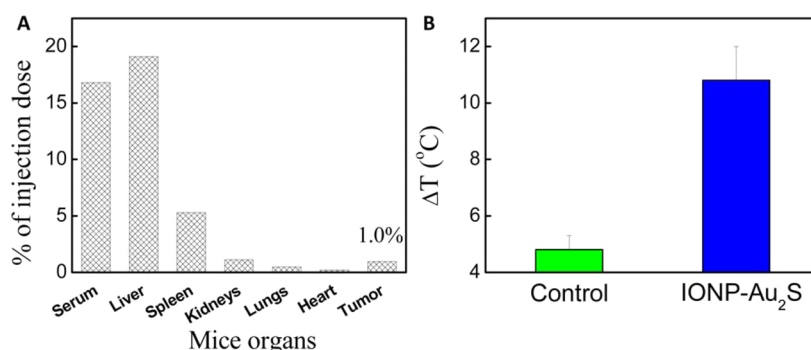
Figure 3. (A) Percentage of injection dose (ID) in main organs at 24 h post intravenous injection with IONP-Au$_2$SNP core—satellite nanomediators based on Au element. The data shown here are already subtracted from the baseline of each organ from PBS control mice (three mice in each group). (B) Surface temperature changes of tumors in mice 24 h post intravenous injection with core—satellite nanomediators or PBS as control after laser irradiation (laser power: 0.5 W) for 10 min (five mice in each group).
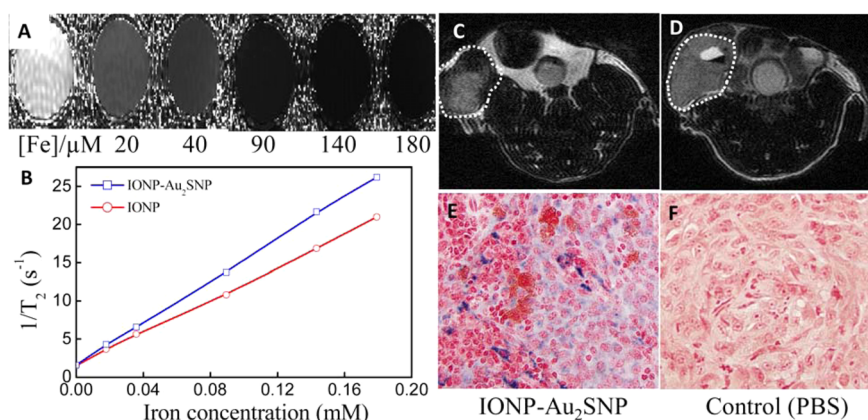
Figure 4. (A) T2-weighted MR images of IONP-Au$_2$SNP core—satellite nanomediator solutions at serial concentrations. (B) T2 relaxation rates (r2) of IONP-Au$_2$SNP core—satellite nanomediators and IONPs in water. MR images of SUM-159 tumor-bearing mice intravenously injected with IONP-Au$_2$SNP core—satellite nanomediators (C) and PBS (D). Circulated areas are tumor sites. Prussian blue staining of tumor tissues from IONP-Au$_2$SNP administered group (E) and control group (F). Images were taken by optical microscopy with 40× objective magnification.

nonspecific binding/uptake by the immune system and thus enhanced tumor accumulation via the EPR effect.

3.1.2. Photothermal Effect of IONP-Au$_2$SNP Nanomediator. To investigate the temperature elevation induced by NIR laser irradiation, we used a continuous-wave diode laser with a center wavelength of 885 nm. Figure 2a shows the temperature profiles for 10 min of laser irradiation of solutions containing IONP−Au$_2$SNP nanomediators, IONPs, or water as a blank control. Our data show that IONP-Au$_2$SNP core—satellite nanomediators significantly enhance the photothermal effect compared to IONPs only. At a nanoparticle concentration of 0.2 mg Fe/mL, the IONP-Au$_2$SNP nanomediator solution (1.0 mL in a cuvette) shows a significant temperature rise from room temperature to 54 °C. Furthermore, the photothermal capability shows no quenching effect for repeated laser on/off cycles as shown in Figure 2b.

In vivo PTT using IONP-Au$_2$SNP core—satellite nanomediators was further demonstrated by human xenograft-bearing immunocompromised mice. Mice bearing SUM-159 tumors were intravenously injected with IONP-Au$_2$SNP nanomediators (with a dose of 20 mg Fe/kg mouse body weight) or PBS as blank control. The biodistribution of the core—satellite nanomediator in tumor-bearing mice (three mice in each group) was first evaluated by analyzing Au concentration in major organs using ICP-OES as shown in Figure 3a. Our data show that the organ distribution is similar based on the metal element analysis of Au from Au$_2$SNPs or Fe from IONPs (Supporting Information Figure S6), suggesting that the core—satellite nanomediator is integrated after circulating in the bloodstream. Our data shows that 24 h post injection ∼1% of the injection dose (ID) accumulates within the tumor, which is comparable to a previous report with PEGylated Au nanorods.[45]

After confirmation of the effective accumulation of the core—satellite nanomediator, tumors were irradiated with the same laser as in the above in vitro solution study but with reduced laser power to minimize potential side effects from laser irradiation alone. The surface temperatures of the tumor sites after laser irradiation were monitored by using an infrared camera as shown in Figure 3b. After laser treatment for 10 min in mice treated with the IONP-Au$_2$SNP nanomediator the tumor surface temperature increases from ∼35 to ∼45.6 °C (Supporting Information Figure S7), with an average tumor temperature increase of 10.8 ± 1.2 °C (five mice per treatment group). In contrast, the surface temperatures of tumors on control mice (treated with PBS plus laser) shows only an increase less than 5 °C after laser irradiation with the same laser power and duration of exposure.

3.1.3. MRI Capability of IONP-Au$_2$SNP Nanomediator. To assess the functionality of the core—satellite nanomediator as a MRI contrast agent we used a 7.4-T MRI system. Figure 4a shows that T2-weighted MR images of the IONP-Au$_2$SNP

Scheme 2. Schematic Illustration of Attaching NIR Dye IR820 to Polysiloxane-Containing Block Copolymer-Coated IONPs
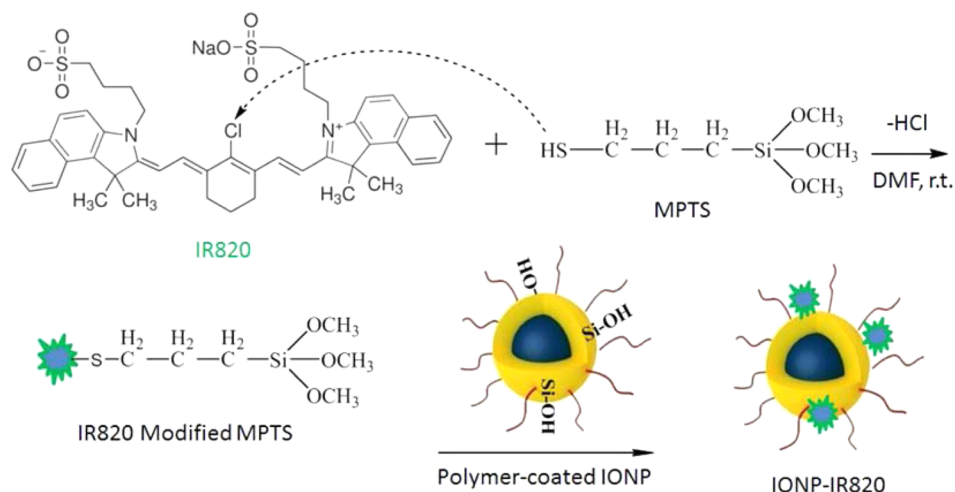
core−satellite nanomediators at increasing iron concentrations from 0 to 180 μM reveal the concentration-dependent darkening effect. Our data show that the transverse relaxivity (r2) slightly enhanced from 107.1 mM^{-1} S^{1-} for IONPs to 137.7 mM^{-1}S^{1-} for IONP-Au$_2$SNPs as shown in Figure 4b. Compared to traditional Au nanoshell-based design, which may block the access of protons to the magnetic core inside, the core−satellite structure does not compromise the MRI contrast effect.[18] The T2-weighted MR imaging capability after intravenous injection of core−satellite nanomediators was further evaluated in SUM-159 tumor-bearing mice. Our imaging data in Figure 4c and 4d show that the darkening effect in tumor tissue is not evenly distributed; instead, the T2-MR signals were significantly decreased at the periphery of the tumor tissue. The intensity changes of the selected areas were quantified by using ImageJ (Supporting Information Figure S8). The data show that the normalized intensity significantly drop by 70% (p-value <0.0001) in selected periphery tumor tissues, but there was no significant signal change deeper within the tumor tissues compared to the control group. The limited tumor tissue penetration is consistent with our previous data and is attributed to the poor vascular structure and higher interstitial fluid pressure inside the tumor tissue.[37,46,47] Overcoming this limitation, which poses a key barrier to the field of nanomedicine, could further improve the enhancement in tumor heating efficiency that we have demonstrated. The presence of IONP-Au$_2$SNPs in tumor tissues was further confirmed by Prussian blue staining of tumor tissue slices as shown in Figure 4e and 4f. The data clearly show that once the nanomediators accumulate at the tumor they were internalized by tumor cells, a beneficial feature for effective photothermal cancer therapy.

3.2. IONP-IR820 Nanomediator for PTT by NIR Laser Irradiation. *3.2.1. Preparation and Characterization of IONP-IR820 Nanomediator.* The organic dye IR820, as an analogue to the Food and Drug Administration-approved indocyanine green (ICG), has strong absorption around 800 nm and has been widely used as an imaging probe and PTT mediator.[27,48] Unlike ICG, IR820 has a reactive chlorine group for further modification.[41,49] Here we modified IR820 with MPTMS to covalently conjugate to polysiloxane-containing polymer-coated IONPs through siloxane chemistry as shown in Scheme 2.

The successful conjugation of siloxane-modified IR820 onto the polysiloxane-containing polymer-coated IONP core was confirmed by the absorption spectra shown in Figure 5a. The
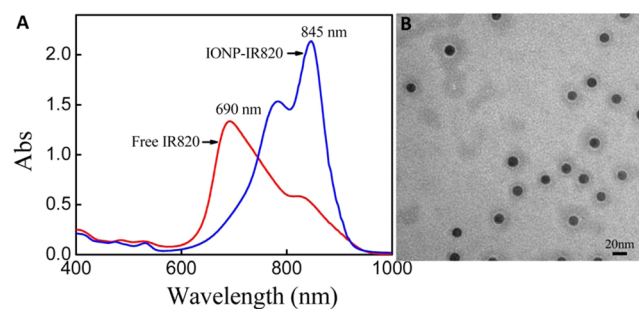

Figure 5. (A) Absorption spectra of IR820 only and IONP-IR820. By measuring the free IR820 concentration in the supernatant, we estimate the IR820 density on each IONP is 2×10^4 IR820 on average. (B) TEM image of IONP-IR820.

purified IONP-IR820 nanomediator has a strong absorption over 700−900 nm that is absent from unmodified IONPs (Supporting Information Figure S3). Compared to free IR820, which has a strongest absorption peak at 690 nm, the highest peak from IONP-IR820 is shifted to 840 nm. This phenomenon is similar to previous findings and is believed to be caused by the formation of an extended Π system by the conjugation process.[50] The density of IR820 on each IONP is quantified through a calibration curve generated by measuring the concentration of the free dye leftover in the supernatant after centrifugation (Supporting Information Figure S9). It is estimated that there are around 2×10^4 IR820 per IONP with a loading capacity at 4.5 mg of IR820/mg of Fe, which is 32 times higher than a recent report of physical encapsulation.[28] The high packing density is probably attributed to the large amount of −SiOH groups from the original IONP polymer coating and also from newly conjugated siloxane-modified IR820. Although it is densely packed with IR820 molecules, the resultant nanomediator's hydrodynamic size as measured by DLS shows little change compared to unmodified IONPs (Supporting Information Table S2). As expected, the zeta potential shows a highly negative surface charge (−57.4 ± 1.2 mV) compared to IONPs only (−14.0 ± 0.3 mV) at pH 8.0 (borate buffer, 50 mM), revealing the existence of negatively charged IR820 on
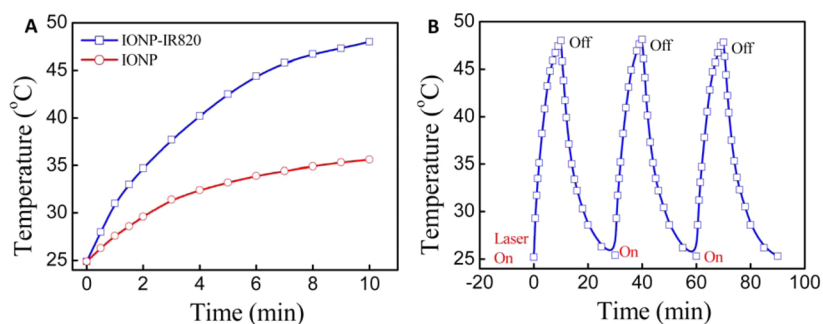
Figure 6. (A) Comparison of photothermal effects of IONP-IR820 and IONPs-only in solutions with a nanoparticle concentration at 0.2 mg Fe/mL, where the laser power is 0.5 W. (B) Temperature changes of IONP-IR820 over three on/off cycles of NIR laser irradiation.
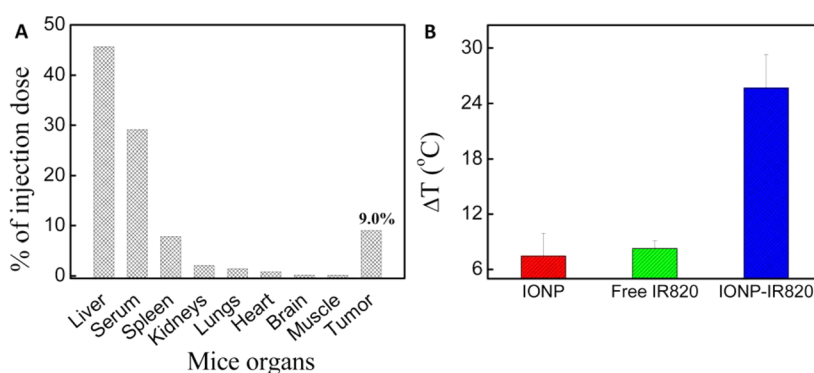

Figure 7. (A) Percentage of injection dose in main organs of SUM-159 tumor-bearing mice at 24 h post intravenous injection of IONP-IR820. The data shown here are already subtracted from the baseline of each organ from PBS control mice (three mice in each group). (B) Surface temperature changes of tumors in mice (24 h post intravenous injection with IONP-IR820 or equal amount of IONP, or free IR820) after laser irradiation for 10 min (five mice in each group). Error bar is standard deviation. Laser power: 0.5 W.

the surface. The TEM image of IONP-IR820 nanomediators in Figure 5b shows that they are individually dispersed and separated from each other, which is consistent with the DLS data.

3.2.2. Enhanced Photothermal Effect of IONP-IR820 Nanomediator Solutions. In our previous publication demonstrating PTT by polymer-coated IONPs without further modification, we used a NIR laser with a power of 1.0 W.[38] To reduce the laser power required to minimize the side effects from laser treatment, we intend to develop new PTT mediators with better photothermal efficiency. Modification with IR820 dramatically enhanced the IONP photothermal effect. First, using the same laser and power as previously described we proved that the IONP-IR820 solution (1.0 mL in a cuvette) temperature increased from 25.2 to 69.0 °C after 10 min of laser irradiation at a nanoparticle concentration of 0.2 mg of Fe/mL (Supporting Information Figure S10), while for the IONP solution the temperature could only be increased to 45.6 °C.[38] Next we showed that using IONPs highly packed with IR820 enables a significant temperature increase at a reduce laser power. Shining the laser at 0.5 W caused the temperature of the same IONP-IR820 solution to reach 48.0 °C, while for IONPs-only solution the temperature was increased to 35.6 °C as shown in Figure 6a. After evaluating the photothermal effect from the other lower laser powers (0.2 and 0.1 W), we chose the laser power at 0.5 W for the following experiments including in vivo studies. Our data in Figure 6b also confirm that IONP-IR820 nanomediators show good photostability against at least three-repeated cycles of laser irradiation. This is consistent with previous work which showed that the

photostability of organic NIR dyes could be improved if they are loaded into micelles.[26,28]

Effective tumor accumulation and in vivo photothermal effect under the NIR light irradiation in tumor-bearing mice after intravenous injection of IONP-IR820 were also proven as shown in Figure 7. Nude mice bearing SUM-159 tumors were injected through tail vein with IONP-IR820 and free IR820 or polymer-coated IONPs as controls. To evaluate the effective accumulation of IONP-IR820 nanomediators, we used ICP-OES to analyze the biodistribution of IONP-IR820 nano-mediators in major organs and serum 24 h post injection as shown in Figure 7a and Supporting Information Figure S11. The data shows that 9% ID of IONP-IR820 was present in tumor tissue, indicating that our IV injected nanomediators can effectively accumulate at tumor tissue by taking advantage of the EPR effect. Such a high tumor accumulation of IONP-IR820 is visible by the naked eye. In mice injected with the IONP-IR820 nanomediators the tumor tissues become blackish before laser treatment; this is not seen in the mice in control groups, as shown in the representative photos (Supporting Information Figure S12, top panel). The tumor accumulation of IONP-IR820 was also confirmed by tissue staining via Prussian blue (Supporting Information Figure S13). Compared to the IONP-Au$_2$SNP core−satellite nanomediator, the enhanced tumor accumulation of IONP-IR820 is believed to be due to the highly charged surface and longer circulation time. This is further revealed by comparing the serum nanoparticle concentration 24 h post injection (Figure 7a and Figure 3a), where the nanoparticle concentration in blood following the injection of IONP-IR820 is much higher than that of IONP-Au$_2$SNP. It is worth noting that very often, nanomediators for
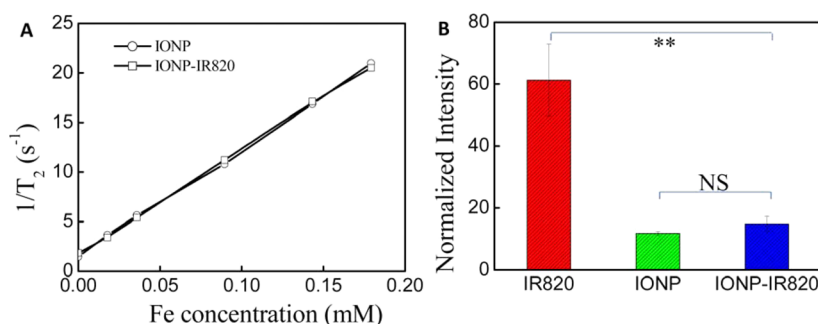
Figure 8. (A) T2 relaxation rates (r2) of IONP and IONP-IR820 solutions at serial concentrations. (B) Normalized T2 weighted intensities in tumor tissues 24 h after tail-vein injection of IONP-IR820 and two controls. ** and NS denote *p*-value <0.005 and no significance, respectively.

PTT are administered through intratumor injection directly to achieve high concentrations locally.[11,17,26,28,29,31,51,52] It is generally believed that nanoparticles with the small overall size and the antibiofouling coating are particularly well suited for effective tumor accumulation via the EPR effect.[24,53] So these small, photostable IONP-IR820 nanomediators may be ideally suited for in vivo PTT to address the challenge of the efficient delivery of nanoparticles to tumor tissue through systemic administration.

Tumors were irradiated with the same NIR laser 24 h post IV injection. For the mice injected with IONP-IR820 tissue hemorrhaging was observed right after laser irradiation for 10 min, revealing the damage of tumor blood vessels by the heated nanoparticles around them (bottom panel in Supporting Information Figure S13). In marked contrast, for the control mice exposed to the laser but only injected with IR820 or IONPs, the tumor tissue does not have any obvious hemorrhaging after laser treatment. The enhanced photothermal effect of the IONP-IR820 nanomediator is shown in Figure 7b. The average temperature increase at the tumor sites in mice treated with IONP-IR820 is 25.7 ± 3.6 °C after laser irradiation for 10 min. In contrast, the surface temperatures of tumors in control treated mice show the average tumor temperature increase of 8.3 ± 0.8 °C for free IR820 and 7.5 ± 2.4 °C for unmodified IONPs, after laser irradiation with the same laser power and duration of exposure. The average temperature increase after laser irradiation for mice injected with IONP-IR820 is ~21 °C higher than that in laser-only control mice injected with PBS. It is worth noting the laser power used in this study is 0.5 W, half of our previous reported laser power.[38] The tissue temperature increase in PBS control mice is significantly reduced, but the heating of tumor tissues from IONP-IR820 treated mice is comparable to our previous treatment using unmodified IONP with laser power at 1.0 W to kill cancer cells.[38] Haematoxylin and eosin (H&E) stained tumor slices further reveal obvious necrosis of tumor tissue immediately following photothermal treatment for the mice injected with IONP-IR820 relative to control normal tumor tissue (Supporting Information Figure S14). The data also suggest that the liver and spleen tissues from the mice injected with IONP-IR820 show little change compared to the control mice based on the H&E staining. These data clearly demonstrate that IONP-IR820 nanocomposites function as effective PTT nanomediators.

3.2.3. MRI Capability of IONP-IR820 Nanomediator. To assess the multimodality properties of as-prepared IONP-IR820, we tested their functionality as a MRI contrast agent through in vitro and in vivo studies as shown in Figure 8. As

expected, the T2-weighted MR images of the nanomediator at increasing concentrations from zero to 180 μM and reveals the concentration-dependent darkening effect enhanced by the IONP-IR820 nanomediator (Supporting Information Figure S15, top panel). Figure 8a shows that, compared to IONP only, there is little change in the measured transverse relaxivity from the IONP core after densely packing with IR820. This was then followed by in vivo evaluation of the T2 weighted MR imaging capability. MR imaging of SUM-159 tumor-bearing mice was conducted after intravenous injection of IR820, IONPs, or IONP-IR820 (Supporting Information Figure S15, bottom panel). Clearly the tumor tissues from the mice administered either IONP-IR820 or IONPs show an obvious darkening effect compared to the control tumor tissue administered with IR820. ImageJ was used to quantitatively compare the signal change in tumor tissues as shown in Figure 8b. The data show that the normalized intensity significantly dropped by 75% ($p < 0.005$) in tumors from mice injected with IONP-IR820 compared to the control mice injected with IR820. This suggests that IONPs densely packed with IR820 could potentially be used as a promising MRI-capable and NIR-resonant nanomediator for photothermal cancer therapy.

4. CONCLUSIONS

In summary, we developed two facile methods to fabricate theranostic nanomediators with a core—satellite structure, based on well-developed polysiloxane-containing polymer-coated IONPs, to impart both MRI and photothermal capabilities. One of the methods is to attach multiple NIR-resonant nanoparticles onto a thiol-modified IONP core through one-step mixing with Au$_2$SNPs. The other strategy is to covalently attach a NIR organic dye onto intact polysiloxane-containing polymer-coated IONPs through facile mixing with siloxane-modified IR820. The successful decoration of the IONP core with either Au$_2$SNPs or IR820 for the resultant nanomediators was demonstrated by using absorption spectra and TEM. It is estimated that around 10 Au$_2$SNPs and 2×10^4 dye molecules (loading capacity: 4.5 mg IR820/mg Fe) are attached onto polymer-coated IONPs. The hydrodynamic sizes of these newly developed multifunctional nanomediators are ~57.5 nm for IONP-Au$_2$SNP and 28.2 nm for IONP-IR820, which are much smaller than traditional Au-nanoshell based designs. The photothermal effects of the IONP-Au$_2$SNP and IONP-IR820 nanomediator solutions under the irradiation of 885 nm NIR laser light have been significantly enhanced compared to IONPs alone. The photothermal effect enhancement by the newly developed nanomediators was also investigated through in vivo studies in nude mice bearing

SUM-159 tumor xenografts. The biodistribution data measured by ICP-OES reveal that ~1% ID of IONP-Au$_2$SNPs and ~9% ID of IONP-IR820 are accumulated into tumor 24 h post intravenous injection at a dose of 20 mg Fe/kg mouse body weight. The average tumor surface temperature recorded by an infrared camera was increased by 10.8 ± 1.2 °C for the mice administered with IONP-Au$_2$SNPs and 25.7 ± 3.6 °C for the group injected with IONP-IR820, compared to 4.8 ± 0.5 °C for the PBS-injected control mice after laser irradiation with a power of 0.5 W for 10 min. Furthermore, our data suggest that the fabrication does not compromise the MRI capability as a contrast agent from the IONP core. Taken together, we demonstrated that NIR-resonant and MRI-capable nano-mediators can be generated without tedious synthesis by using polysiloxane-containing polymer-coated IONPs as the core. The as-developed theranostic nanomediators could potentially be used for photothermal cancer therapy coupled with the ability to locate the tumor and monitor the therapeutic effect noninvasively.

■ ASSOCIATED CONTENT

ⓢ Supporting Information

Structure of polysiloxane-containing polymer for coating IONP, optical absorption spectra of nanoparticles, representative photos taken by infrared camera, quantification of IR820 density on nanoparticle, and T2-weighted MR images of IONP-IR820. The Supporting Information is available free of charge on the ACS Publications website at DOI: 10.1021/acsami.5b01991.

■ AUTHOR INFORMATION

Corresponding Authors
*E-mail: duxins@umich.edu.
*E-mail: hongweic@umich.edu.
Author Contributions
#These authors contribute equally to this work

Author Contributions

The manuscript was written through contributions of all authors. All authors have given approval to the final version of the manuscript. These authors contribute equally to this work

Notes

The authors declare no competing financial interest.

■ ACKNOWLEDGMENTS

■ REFERENCES

(1) Cherukuri, P.; Glazer, E. S.; Curleya, S. A. Targeted Hyper-thermia Using Metal Nanoparticles. *Adv. Drug Delivery Rev.* **2010**, *62*, 339−345.

(2) Yang, K.; Feng, L. Z.; Shi, X. Z.; Liu, Z. Nano-Graphene in Biomedicine: Theranostic Applications. *Chem. Soc. Rev.* **2013**, *42*, 530−547.

(3) Melancon, M. P.; Zhou, M.; Li, C. Cancer Theranostics with Near-Infrared Light-Activatable Multimodal Nanoparticles. *Acc. Chem. Res.* **2011**, *44*, 947−956.

(4) Kennedy, L. C.; Bickford, L. R.; Lewinski, N. A.; Coughlin, A. J.; Hu, Y.; Day, E. S.; West, J. L.; Drezek, R. A. A New Era for Cancer Treatment: Gold-Nanoparticle-Mediated Thermal Therapies. *Small* **2011**, *7*, 169−183.

(5) Cheng, L.; Wang, C.; Feng, L.; Yang, K.; Liu, Z. Functional Nanomaterials for Phototherapies of Cancer. *Chem. Rev.* **2014**, *114*, 10869−939.

(6) Guo, L. R.; Yan, D. D.; Yang, D. F.; Li, Y. J.; Wang, X. D.; Zalewski, O.; Yan, B. F.; Lu, W. Combinatorial Photothermal and Immuno Cancer Therapy Using Chitosan-Coated Hollow Copper Sulfide Nanoparticles. *ACS Nano* **2014**, *8*, 5670−5681.

(7) Bear, A. S.; Kennedy, L. C.; Young, J. K.; Perna, S. K.; Almeida, J. P. M.; Lin, A. Y.; Eckels, P. C.; Drezek, R. A.; Foster, A. E. Elimination of Metastatic Melanoma Using Gold Nanoshell-Enabled Photothermal Therapy and Adoptive T Cell Transfer. *PLoS One* **2013**, *8*, No. e69073.

(8) Reginato, E.; Mroz, P.; Chung, H.; Kawakubo, M.; Wolf, P.; Hamblin, M. R. Photodynamic Therapy Plus Regulatory T-Cell Depletion Produces Immunity Against a Mouse Tumour That Expresses a Self-Antigen. *Br. J. Cancer* **2013**, *109*, 2167−2174.

(9) Castano, A. P.; Mroz, P.; Wu, M. X.; Hamblin, M. R. Photodynamic Therapy Plus Low-Dose Cyclophosphamide Generates Antitumor Immunity in a Mouse Model. *Proc. Natl. Acad. Sci. USA* **2008**, *105*, 5495−5550.

(10) Ke, H. T.; Wang, J. R.; Dai, Z. F.; Jin, Y. S.; Qu, E. Z.; Xing, Z. W.; Guo, C. X.; Yue, X. L.; Liu, J. B. Gold-Nanoshelled Microcapsules: A Theranostic Agent for Ultrasound Contrast Imaging and Photo-thermal Therapy. *Angew. Chem., Int. Ed.* **2011**, *50*, 3017−3021.

(11) Hirsch, L. R.; Stafford, R. J.; Bankson, J. A.; Sershen, S. R.; Rivera, B.; Price, R. E.; Hazle, J. D.; Halas, N. J.; West, J. L. Nanoshell-Mediated Near-Infrared Thermal Therapy of Tumors under Magnetic Resonance Guidance. *Proc. Natl. Acad. Sci. USA* **2003**, *100*, 13549−13554.

(12) Kuo, W. S.; Chang, C. N.; Chang, Y. T.; Yang, M. H.; Chien, Y. H.; Chen, S. J.; Yeh, C. S. Gold Nanorods in Photodynamic Therapy, as Hyperthermia Agents, and in Near-Infrared Optical Imaging. *Angew. Chem., Int. Ed.* **2010**, *49*, 2711−2715.

(13) Huang, X.; El-Sayed, I. H.; Qian, W.; El-Sayed, M. A. Cancer Cell Imaging and Photothermal Therapy in the Near-Infrared Region by Using Gold Nanorods. *J. Am. Chem. Soc.* **2006**, *128*, 2115−2120.

(14) Yavuz, M. S.; Cheng, Y. Y.; Chen, J. Y.; Cobley, C. M.; Zhang, Q.; Rycenga, M.; Xie, J. W.; Kim, C.; Song, K. H.; Schwartz, A. G.; Wang, L. H. V.; Xia, Y. N. Gold Nanocages Covered by Smart Polymers for Controlled Release with Near-Infrared Light. *Nat. Mater.* **2009**, *8*, 935−939.

(15) Averitt, R. D.; Westcott, S. L.; Halas, N. J. Ultrafast Optical Properties of Gold Nanoshells. *J. Opt. Soc. Am. B* **1999**, *16*, 1814−1823.

(16) Gobin, A. M.; Watkins, E. M.; Quevedo, E.; Colvin, V. L.; West, J. L. Near-Infrared-Resonant Gold/Gold Sulfide Nanoparticles as a Photothermal Cancer Therapeutic Agent. *Small* **2010**, *6*, 745−752.

(17) Dong, W. J.; Li, Y. S.; Niu, D. C.; Ma, Z.; Gu, J. L.; Chen, Y.; Zhao, W. R.; Liu, X. H.; Liu, C. S.; Shi, J. L. Facile Synthesis of Monodisperse Superparamagnetic Fe$_3$O$_4$ Core@Hybrid@Au Shell Nanocomposite for Bimodal Imaging and Photothermal Therapy. *Adv. Mater.* **2011**, *23*, 5392−5397.

(18) Ji, X. J.; Shao, R. P.; Elliott, A. M.; Stafford, R. J.; Esparza-Coss, E.; Bankson, J. A.; Liang, G.; Luo, Z. P.; Park, K.; Markert, J. T.; Li, C. Bifunctional Gold Nanoshells with a Superparamagnetic Iron Oxide−Silica Core Suitable for both MR Imaging and Photothermal Therapy. *J. Phys. Chem. C* **2007**, *111*, 6245−6251.

(19) Zhang, Q.; Ge, J. P.; Goebl, J.; Hu, Y. X.; Sun, Y. G.; Yin, Y. D. Tailored Synthesis of Superparamagnetic Gold Nanoshells with Tunable Optical Properties. *Adv. Mater.* **2010**, *22*, 1905−1909.

(20) Fan, Z.; Shelton, M.; Singh, A. K.; Senapati, D.; Khan, S. A.; Ray, P. C. Multifunctional Plasmonic Shell-Magnetic Core Nanoparticles for Targeted Diagnostics, Isolation, and Photothermal Destruction of Tumor Cells. *ACS Nano* **2012**, *6*, 1065−1073.

(21) Jaque, D.; Maestro, L. M.; del Rosal, B.; Haro-Gonzalez, P.; Benayas, A.; Plaza, J. L.; Rodriguez, E. M.; Sole, J. G. Nanoparticles for Photothermal Therapies. *Nanoscale* **2014**, *6*, 9494−9530.

(22) Fu, G. L.; Liu, W.; Li, Y. Y.; Jin, Y. S.; Jiang, L. D.; Liang, X. L.; Feng, S. S.; Dai, Z. F. Magnetic Prussian Blue Nanoparticles for Targeted Photothermal Therapy under Magnetic Resonance Imaging Guidance. *Bioconjugate Chem.* **2014**, *25*, 1655−1663.

(23) Yang, K.; Hu, L. L.; Ma, X. X.; Ye, S. Q.; Cheng, L.; Shi, X. Z.; Li, C. H.; Li, Y. G.; Liu, Z. Multimodal Imaging Guided Photothermal Therapy using Functionalized Graphene Nanosheets Anchored with Magnetic Nanoparticles. *Adv. Mater.* **2012**, *24*, 1868−1872.

(24) Cabral, H.; Matsumoto, Y.; Mizuno, K.; Chen, Q.; Murakami, M.; Kimura, M.; Terada, Y.; Kano, M. R.; Miyazono, K.; Uesaka, M.; Nishiyama, N.; Kataoka, K. Accumulation of Sub-100 nm Polymeric Micelles in Poorly Permeable Tumours Depends on Size. *Nat. Nanotechnol.* **2011**, *6*, 815−823.

(25) Yue, C. X.; Liu, P.; Zheng, M. B.; Zhao, P. F.; Wang, Y. Q.; Ma, Y. F.; Cai, L. T. IR-780 Dye Loaded Tumor Targeting Theranostic Nanoparticles for NIR Imaging and Photothermal Therapy. *Biomaterials* **2013**, *34*, 6853−6861.

(26) Zheng, X. H.; Zhou, F. F.; Wu, B. Y.; Chen, W. R.; Xing, D. Enhanced Tumor Treatment Using Biofunctional Indocyanine Green-Containing Nanostructure by Intratumoral or Intravenous Injection. *Mol. Pharmaceut.* **2012**, *9*, 514−522.

(27) Fernandez-Fernandez, A.; Manchanda, R.; Lei, T. J.; Carvajal, D. A.; Tang, Y.; Kazmi, S. Z. R.; McGoron, A. J. Comparative Study of the Optical and Heat Generation Properties of IR820 and Indocyanine Green. *Mol. Imaging* **2012**, *11*, 99−113.

(28) Ma, Y.; Tong, S.; Bao, G.; Gao, C.; Dai, Z. F. Indocyanine Green Loaded SPIO Nanoparticles with Phospholipid-PEG Coating for Dual-Modal Imaging and Photothermal Therapy. *Biomaterials* **2013**, *34*, 7706−7714.

(29) Cheng, L.; He, W. W.; Gong, H.; Wang, C.; Chen, Q.; Cheng, Z. P.; Liu, Z. PEGylated Micelle Nanoparticles Encapsulating a Non-Fluorescent Near-Infrared Organic Dye as a Safe and Highly-Effective Photothermal Agent for In Vivo Cancer Therapy. *Adv. Funct. Mater.* **2013**, *23*, 5893−5902.

(30) Tian, Q. W.; Hu, J. Q.; Zhu, Y. H.; Zou, R. J.; Chen, Z. G.; Yang, S. P.; Li, R. W.; Su, Q. Q.; Han, Y.; Liu, X. G. Sub-10 nm Fe$_3$O$_4$@ Cu$_{2−x}$S Core-Shell Nanoparticles for Dual-Modal Imaging and Photothermal Therapy. *J. Am. Chem. Soc.* **2013**, *135*, 8571−8577.

(31) Wang, C.; Xu, H.; Liang, C.; Liu, Y. M.; Li, Z. W.; Yang, G. B.; Cheng, H.; Li, Y. G.; Liu, Z. Iron Oxide @ Polypyrrole Nanoparticles as a Multifunctional Drug Carrier for Remotely Controlled Cancer Therapy with Synergistic Antitumor Effect. *ACS Nano* **2013**, *7*, 6782−6795.

(32) Lee, H.; Lee, E.; Kim, D. K.; Jang, N. K.; Jeong, Y. Y.; Jon, S. Antibiofouling Polymer-Coated Superparamagnetic Iron Oxide Nanoparticles as Potential Magnetic Resonance Contrast Agents for In Vivo Cancer Imaging. *J. Am. Chem. Soc.* **2006**, *128*, 7383−7389.

(33) Lee, H.; Yu, M. K.; Park, S.; Moon, S.; Min, J. J.; Jeong, Y. Y.; Kang, H. W.; Jon, S. Thermally Cross-Linked Superparamagnetic Iron Oxide Nanoparticles: Synthesis and Application as a Dual Imaging Probe for Cancer In Vivo. *J. Am. Chem. Soc.* **2007**, *129*, 12739−12745.

(34) Chen, H. W.; Wu, X. Y.; Duan, H. W.; Wang, Y. A.; Wang, L. Y.; Zhang, M. M.; Mao, H. Biocompatible Polysiloxane-Containing Diblock Copolymer PEO-*b*-PγMPS for Coating Magnetic Nanoparticles. *ACS Appl. Mater. Interfaces* **2009**, *1*, 2134−2140.

(35) Chen, H. W.; Wang, L. Y.; Yeh, J.; Wu, X. Y.; Cao, Z. H.; Wang, Y. A.; Zhang, M. M.; Yang, L.; Mao, H. Reducing Non-Specific Binding and Uptake of Nanoparticles and Improving Cell Targeting with an Antifouling PEO-*b*-PγMPS Copolymer Coating. *Biomaterials* **2010**, *31*, 5397−5407.

(36) Chen, H. W.; Yeh, J. L.; Wang, L. Y.; Khurshid, H.; Peng, N.; Wang, A. Y.; Mao, H. Preparation and Control of the Formation of Single Core and Clustered Nanoparticles for Biomedical Applications Using a Versatile Amphiphilic Diblock Copolymer. *Nano Res.* **2010**, *3*, 852−862.

(37) Chen, H.; Wang, L.; Yu, Q.; Qian, W.; Tiwari, D.; Yi, H.; Wang, A. Y.; Huang, J.; Yang, L.; Mao, H. Anti-HER2 Antibody and ScFvEGFR-Conjugated Antifouling Magnetic Iron Oxide Nano-

particles for Targeting and Magnetic Resonance Imaging of Breast Cancer. *Int. J. Nanomedicine* **2013**, *8*, 3781−3794.

(38) Chen, H. W.; Burnett, J.; Zhang, F. X.; Zhang, J. M.; Paholak, H.; Sun, D. X. Highly Crystallized Iron Oxide Nanoparticles as Effective and Biodegradable Mediators for Photothermal Cancer Therapy. *J. Mater. Chem. B* **2014**, *2*, 757−765.

(39) Sun, X. H.; Zhang, G. D.; Patel, D.; Stephens, D.; Gobin, A. M. Targeted Cancer Therapy by Immunoconjugated Gold−Gold Sulfide Nanoparticles Using Protein G as a Cofactor. *Ann. Biomed. Eng.* **2012**, *40*, 2131−2139.

(40) Li, Y.; Gobin, A. M.; Dryden, G. W.; Kang, X. Q.; Xiao, D. Y.; Li, S. P.; Zhang, G. D.; Martin, R. C. G. Infrared Light-Absorbing Gold/ Gold Sulfide Nanoparticles Induce Cell Death in Esophageal Adenocarcinoma. *Int. J. Nanomed.* **2013**, *8*, 2153−2161.

(41) Strekowski, L.; Mason, C. J.; Lee, H.; Gupta, R.; Sowell, J.; Patonay, G. Synthesis of Water-Soluble Near-Infrared Cyanine Dyes Functionalized with [(Succinimido)Oxy]Carbonyl Group. *J. Heterocyclic Chem.* **2003**, *40*, 913−916.

(42) Tang, L.; Fan, T. M.; Borst, L. B.; Cheng, J. Synthesis and Biological Response of Size-Specific, Monodisperse Drug−Silica Nanoconjugates. *ACS Nano* **2012**, *6*, 3954−3966.

(43) Melancon, M. P.; Lu, W.; Zhong, M.; Zhou, M.; Liang, G.; Elliott, A. M.; Hazle, J. D.; Myers, J. N.; Li, C.; Stafford, R. J. Targeted Multifunctional Gold-Based Nanoshells for Magnetic Resonance-Guided Laser Ablation of Head and Neck Cancer. *Biomaterials* **2011**, *32*, 7600−7608.

(44) Schwartzberg, A. M.; Grant, C. D.; van Buuren, T.; Zhang, J. Z. Reduction of HAuCl$_4$ by Na$_2$S Revisited: The Case for Au Nanoparticle Aggregates and Against Au$_2$S/Au Core/Shell Particles. *J. Phys. Chem. C* **2007**, *111*, 8892−8901.

(45) Huang, X. H.; Peng, X. H.; Wang, Y. Q.; Wang, Y. X.; Shin, D. M.; El-Sayed, M. A.; Nie, S. M. A Reexamination of Active and Passive Tumor Targeting by Using Rod-Shaped Gold Nanocrystals and Covalently Conjugated Peptide Ligands. *ACS Nano* **2010**, *4*, 5887−5896.

(46) Yuan, F.; Leunig, M.; Huang, S. K.; Berk, D. A.; Papahadjopoulos, D.; Jain, R. K. Microvascular Permeability and Interstitial Penetration of Sterically Stabilized (Stealth) Liposomes in a Human Tumor Xenograft. *Cancer Res.* **1994**, *54*, 3352−3356.

(47) Boucher, Y.; Baxter, L. T.; Jain, R. K. Interstitial Pressure-Gradients in Tissue-Isolated and Subcutaneous Tumors—Implications for Therapy. *Cancer Res.* **1990**, *50*, 4478−4484.

(48) Zheng, C. F.; Zheng, M. B.; Gong, P.; Jia, D. X.; Zhang, P. F.; Shi, B. H.; Sheng, Z. H.; Ma, Y. F.; Cai, L. T. Indocyanine Green-Loaded Biodegradable Tumor Targeting Nanoprobes for In Vitro and In Vivo Imaging. *Biomaterials* **2012**, *33*, 5603−5609.

(49) Tang, L.; Fan, T. M.; Borst, L. B.; Cheng, J. J. Synthesis and Biological Response of Size-Specific, Monodisperse Drug−Silica Nanoconjugates. *ACS Nano* **2012**, *6*, 3954−3966.

(50) Fernandez-Fernandez, A.; Manchanda, R.; Carvajal, D. A.; Lei, T.; Srinivasan, S.; McGoron, A. J. Covalent IR820-PEG-Diamine Nanoconjugates for Theranostic Applications in Cancer. *Int. J. Nanomed.* **2014**, *9*, 4631−4648.

(51) Chu, M. Q.; Shao, Y. X.; Peng, J. L.; Dai, X. Y.; Li, H. K.; Wu, Q. S.; Shi, D. L. Near-Infrared Laser Light Mediated Cancer Therapy by Photothermal Effect of Fe$_3$O$_4$ Magnetic Nanoparticles. *Biomaterials* **2013**, *34*, 4078−4088.

(52) Gu, L.; Vardarajan, V.; Koymen, A. R.; Mohanty, S. K. Magnetic-Field-Assisted Photothermal Therapy of Cancer Cells Using Fe-Doped Carbon Nanoparticles. *J. Biomed. Opt.* **2012**, *17*, 018003.

(53) Zhang, G. D.; Yang, Z.; Lu, W.; Zhang, R.; Huang, Q.; Tian, M.; Li, L.; Liang, D.; Li, C. Influence of Anchoring Ligands and Particle Size on the Colloidal Stability and In Vivo Biodistribution of Polyethylene Glycol-Coated Gold Nanoparticles in Tumor-Xeno-grafted Mice. *Biomaterials* **2009**, *30*, 1928−1936.